High Efficiency Thermoelectric Temperature Control System With Improved Proportional Integral differential (PID) Algorithm Using Energy Feedback Technique

Ning Wang, Member, IEEE, Zhou Xiao Liu, Can Ding, Member, IEEE, Jian-Nan Zhang, Guo-Rong Sui, Senior Member, IEEE, Hong-Zhi Jia, and Xiu-Min Gao

***Abstract*—This paper proposes an efficient thermoelectric temperature control system based on an improved proportional integral differential (PID) algorithm in which energy feedback technology is used to enhance thermoelectric cooling. In the proposed power management system, two groups of batteries are efficiently and alternatingly charged and discharged such that the information of the circuit can be monitored in real time. The PID algorithm is improved by using the idea of a state machine to control the thermoelectric coolers (TEC) through an H-bridge circuit with pulse-width modulation. Finally, the energy feedback circuit combined with improved synchronous switching technology is designed to recycle the energy to drive the sensor. By inputting current of 3.1 A, a wide range of temperature control from 1.437 ℃ to 60.187 ℃ was implemented. While targeting a temperature of 10 ℃ at an ambient temperature of 22 ℃, the proposed temperature control system had a control time of 30.5 s, compared with 287 s when using the conventional method, with an accuracy of 0.1 ℃, and an error of only ±0.35 ℃. The results confirm that electric energy at a peak voltage of 1.2 V and current of 24 μA can be recovered. The proposed energy feedback system can thus improve the efficiency of energy utilization of TEC from a peripheral circuit.**

***Index Terms*—Temperature control system, thermoelectric cooling, PID algorithm, energy feedback, energy harvesting**

I. Introduction

With the development of the modern electronics industry, the demand for thermal dissipation is increasing [1-5].

Manuscript received; This work was supported in part by NSFC under Grant 61804096, in part by the National Key Research and Development Plan--Earth Observation and Navigation Key Special Project under Grant 2017YFB0503102, in part by the National Key Research and Development Program of China under Grant 2018YFC1313803 and 2018YFA0701800. (Corresponding author: Can Ding)

N. Wang, Z.-X. Liu, J.-N. Zhang, G.-R. Sui, H.-Z. Jia and X.-M. Gao are with the Engineering Research Center of Optical Instrument and System, Ministry of Education, Shanghai Key Laboratory of Modern Optical System, University of Shanghai for Science and Technology, Shanghai 200093, China (e-mail: nwang@usst.edu.cn, 182390274@st.usst.edu.cn, 192380329@st.usst.edu.cn, suigr@usst.edu.cn, hzjia@usst.edu.cn, gxm@usst.edu.cn).

C. Ding is with the Global Big Data Technologies Center, University of Technology Sydney, Sydney, NSW 2007, Australia (e-mail: Can.Ding@uts.edu.au).

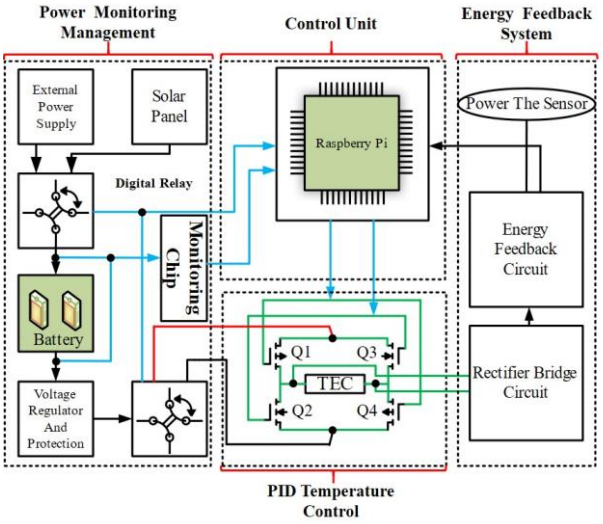

Fig. 1. Diagram of system composition.

For example, with improvements in the chip manufacturing process, heat dissipation has emerged as a significant problem that restricts the development of high-performance chips and large power dissipation devices [6-11].

On the contrary, the requirements for safe, miniature, and accurate temperature control in various applications are becoming increasingly stringent [12,13]. Electric energy can be converted into thermal energy by a thermoelectric cooler (TEC) based on the Peltier effect, which is generally used to cool large power devices and is applied to attain precise temperature control [14-19]. Due to the advantages of TEC over conventional cooling methods, including solid-state operation, absence of toxic residuals, scalability, maintenance-free operation, and long lifespan of reliable operation, TEC offers a great solution of temperature control as a semiconductor refrigeration device in many scenarios [20-21].

Compared with conventional temperature control technologies, where heating or cooling are often discerte and one-directional, the semiconductor temperature control system based on TEC is bidirectional, i.e., it can convert heating and cooling by reversing the current flowing through TEC [22-24]. However, commercial applications of TEC are limited by the relatively low efficiency of energy conversion of between 5% and 10% [1,3]. To improve the conversion efficiency, the research has mainly focused on the development of high-efficiency hot structures and materials in recent years [25-30]. In addition, a few attempts have been made to improve the

cooling efficiency of the TEC in terms of energy feedback to implement power generation together with other power sources, such as photovoltaic cells, from the perspective of application. A wide temperature range and fast temperature control response have also garnered attention in temperature control systems. By using a proportional integral differential (PID) compensation network, a temperature control system was implemented on ranges of the TEC from 5 ℃ to 55 ℃ by continuously adjusting the accuracy to as high as 0.5 ℃ in [22]. In [24], the cooling process was accelerated three times by using the PID temperature control of a thermoelectric cooler box where the temperature could be reduced to 11 ℃ within 2060 s. Engelmann used the TEC [31] to propose a temperature control algorithm that can achieve short settling times without overshoot. However, the results showed that maintaining a steady-state temperature during the cooling process takes 300 s when two heat sinks are fed directly into the modulator. Most available temperature control systems based on TEC are limited by their control algorithms. As a result, the realized temperature control is not fast enough, and features large temperature fluctuations and long regulation time.

In this paper, an efficient thermoelectric temperature control system is designed that can recycle the reverse Seebeck voltage by using a TEC. By using the intelligent charging and discharging management of power supply, a new temperature control algorithm with fast response and efficient energy feedback mechanism for TEC is obtained. This work can put forward a new scheme on temperature control for some special application scenarios such as portable equipment, space power supply, low power industrial control and automotive electronics. The remainder of this paper is organized as follows. In Section II, the theoretical basis of the proposed scheme is detailed and the principle of temperature control is presented. Section III describes the design of the proposed scheme and a simulation of energy feedback applied to the TEC refrigeration process. Section IV explains the system module and control software. The performance of the proposed system is experimentally evaluated and discussed in Section V, and Section VI gives the conclusions of this work.

II. System Design

A block diagram of the proposed temperature control system is shown in Fig. 1. It generally consists of four modules: a power monitoring and management (PMM) module, a PID temperature control module, an energy feedback module, and a control unit.

The PMM module includes an external power supply and a solar panel for charging, both of which can be controlled by computer software through a digital relay. This allows the system to continue charging and discharging at the same time. Two power consumption monitoring chips are employed in this module to assess the charging and discharging of the two batteries in real time. The chips communicate with the host computer to intelligently switch the batteries on and off. Additionally, to ensure that the charging process is smooth and safe, a voltage regulation part was also employed on the PWM module.

The PID temperature control module employs a TEC together with four metal-oxide-semiconductor field-effect transistors (MOSFETs) to cooperatively control the temperature of the TEC. In the central control unit, an improved PID algorithm based on Raspberry Pi is embedded, which is a combination of a state machine and a conventional PID algorithm. In the energy feedback module, there is a rectifier bridge circuit to recycle electrical energy and use it to power sensors of the system. Electrical energy is produced when there is a large temperature difference between the top and bottom surfaces of the TEC. The collected electrical energy can drive the sensor in the system through a boost circuit, which improves the cooling efficiency of the TEC.

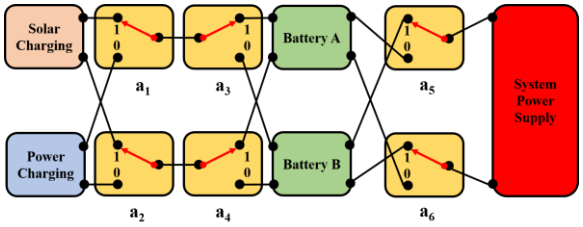

Fig. 2. Diagram of control circuit.

TABLE I
STATE MODE OF CHARGE AND DISCHARGE SWITCHING

	A charging (or disconnected), B discharging	B charging (or disconnected), A discharging
Solar Charging	111111	110000
Power Charging	001111	000000

Algorithm 1 Intelligent control algorithm of dual power charge and discharge

Input: Q_a, Q_b: real quantity for batteries A and B; I_c: charging currents; I_d:discharging current.

Output: O: The six-bit logic level signal output by the upper computer.

Initial: set the battery's capacity Q_c, minimum current of solar charging i_m.

repeat:

if $q_b \geqslant q_c$ **or** i_d=0:

if $i_c > i_m$: o=110000;

else: o=000000;

else if $q_a \geqslant q_c$ **or** i_d=0**:**

if $i_c > i_m$: o=111111;

else: o=001111;

until (interrupt instruction received)

A. System Charging Scheme

A combination of solar charging and electrical energy charging is used in the system, with the former acts as the main scheme and the latter as the alternative scheme. The system is equipped with two sets of batteries, one for discharging and the other for charging. The choice of charging scheme is controlled by the computer through the digital relay module. The current, power, and voltage of the charging and discharging processes can be obtained by the computer in real time through the current monitoring chip. The electric intensity of the discharging and charging groups can be similarly determined, and the charging and discharging statement is automatically switched through the digital relays.

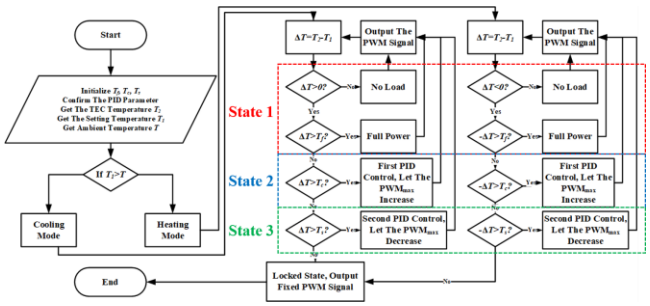

Fig. 3. Flowchart of the improved algorithm that combines the PID algorithm and state machine control with three states.

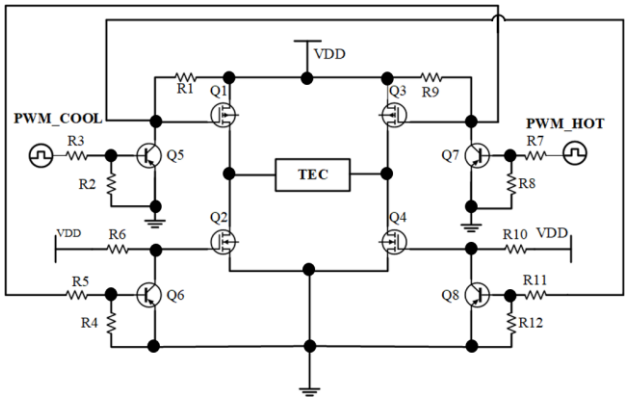

Fig. 4. H-bridge control circuit.

In this way, continuous charging and discharging can be carried out, resulting in highly efficient solar charging that saves energy. Six digital relays are set to control the statement, and are controlled in turn by Raspberry Pi. The output digital signal can be switched on through output logic level signal as shown in Fig. 2. It can be seen from Fig. 2 that when the control system inputs 1 to relays a_1, a_2, a_3, a_4, a_5 and a_6 at the same time, the state is photovoltaic charging. At this time, batteries in group A charge and batteries in group B discharge. The corresponding signal inputs for the remaining states are listed in Table I. The control pseudocode is shown in Algorithm 1.

B. Design of Improved PID Control Algorithm and Circuit Scheme

In order to realize the controlled current of TEC, Pulse Width Modulation (PWM) technology is adopted. Using this technology, the bias of base of a transistor or gate of a MOS tube will be modulated to change their conduction time and output of switching regulated power supply according to load changes. In our proposed system, the duty cycle of PWM wave is controlled by the improved PID algorithm.

The PID algorithm is controlled according to the proportion, integral, and differential, where this is widely used in the control of continuous systems. PID algorithms can be divided into two types: position and incremental PID algorithms. The incremental PID algorithm is used in our work. The laws of the two control calculations are defined as (1) and (2), respectively:

$$OUT_K = K_P(e_k + \frac{T}{T_I}\sum_{K=1}^{n} e_k + \frac{T_D}{T}(e_k - e_{k-1})) \quad (1)$$

$$\Delta OUT_K = K_P[(e_k - e_{k-1}) + \frac{T}{T_I}e_k + \frac{T_D}{T}(e_k - 2e_{k-1} + e_{k-2})] \quad (2)$$

where K_p, T, T_I, and T_D are, respectively, the proportional coefficient, regulation period, integral regulation period, and differential regulation period; e_k, e_{k-1}, and e_{k-2} are the kth error, the k-1th error, and the k-2th error, respectively.

Owing to the thermal conductivity of the thermal medium which cannot be ignored, heat conduction has the characteristics of hysteresis and inertia. When the conventional PID feedback adjustment is directly applied to the temperature control of the TEC, a long regulation time is needed and large temperature fluctuations occur in the regulation process. By combining the control mode of the state machine with the conventional PID algorithm, the problems of a long starting time and overshooting in the conventional PID feedback regulation can be avoided, as can overcoming the state callback caused by the single judgment condition in the conventional control algorithm and the endless loop in the control process. The flow of the proposed algorithm is shown in Fig. 3 and the relevant description is provided in Table II.

The temperature of the TEC and the ambient temperature is first measured and transmitted by temperature sensor, then the target temperature is set and the working mode to be executed is determined. Three special temperature differences T_f, T_c, and T_s are set, where T_f>T_c>T_s are the temperature difference threshold of the first adjustment judgment, the temperature difference threshold of the second adjustment judgment, and the temperature difference threshold of the control stop judgment, respectively.

When the difference between the given temperature and the set temperature is greater than T_f, the system is judged to deviate significantly from the set temperature. The current is then adjusted to its maximum value so that the TEC operates at maximum power, and the temperature at the test point drops sharply (rises sharply). When the difference between the given temperature and the set temperature is less than T_f and greater than T_c, the system is judged to be in the transition phase of State 2, and a higher value of the output of the maximum pulse-width modulation (PWM) is set as the buffer. The temperature of the measuring point is gradually adjusted toward the target temperature. When the given temperature is less than T_c and greater than T_s, the temperature of the system is near the expected temperature, and the value of T_s leads to the setting of an appropriate maximum value of the PWM to adjust the PID

Algorithm 2 Anti-windup mechanism in state control

Output: current_state;
Input: T_a: ambient temperature, T_t: target temperature;
Initial T_f,T_c,T_s;
define e as $|T_a - T_t|$;
repeat:
$flag\_f$ = 0,$flag\_c$ = 0,$flag\_s$ = 0;
if $e > T_f$ **and** $flag\_c$ = 0 **and** $flag\_s$ = 0:
$current\_state = state\_1$;
$flag\_f$ = 1;
if $T_c < e < T_f$ **and** $flag\_s$ = 0:
$current\_state = state\_2$;
$flag\_c$ = 1;
if $e<T_s$:
$current\_state=state\_3$;
$flag\_s$ = 1;
until (Interrupt instruction received)

TABLE Ⅲ
Parameters of circuit

Symbol	Device	Value
Q1, Q4	IRF5210	/
Q2, Q3	MTP50N05EL	/
R1, R6, R9, R10	Resistor	1 kΩ
Q5, Q6, Q7, Q8	2N1711	/
R3, R5, R7, R11	Resistor	10 Ω
R2, R4, R8, R12	Resistor	10 kΩ
VDD	Power	12 V

feedback. After fine-tuning the temperature of the measuring point, the temperature floating up and down the target temperature and gradually pushing towards the target temperature. When the temperature is less than T_s in successive adjustment cycles, the system is determined to be stable at the desired temperature, and the adjustments are stopped.

In the control code, three flag bits are set as the judgment conditions for the entry of three states. The existence of three state flag bits makes the entry of three states not depend solely on the condition judgment of temperature, but add a logic: the next state cannot jump into the previous state. By setting the flag bit as the necessary condition of state jump, the dead loop caused by state callback can be avoided. The anti-windup mechanism's pseudocode is shown in Algorithm 2, where state_1, state_2, state_3 correspond to the control stages marked in Fig. 3, respectively.

In each control period, Raspberry Pi uses algorithmic calculations to output the PWM control signal, and controls the current and direction of the TEC through the H-bridge circuit as shown in Fig. 4. When the system is in cooling mode, the PWM control signal is connected to the PWM_COOL port and the PWM_HOT signal port is suspended. Similarly, when the system is in heat mode, the PWM_COOL port is suspended and the control signal is connected to the PWM_HOT port. When the PWM_COOL port receives the PWM signal, Q1 and Q4 are switched to a high level and closed at a low level in a signal cycle, thus realizing the control of the TEC current with PWM signals of different duty ratios. The parameters of the circuit device are listed in Table III.

III. ENERGY FEEDBACK SYSTEM OF TEC

Energy feedback technology is applied to the TEC in this paper for the first time. By using the energy feedback device, the reverse Seebeck energy generated during the no-load period of the TEC in PWM control is recovered to power the sensors. Therefore, the energy per unit time consumed by the TEC temperature control system is reduced, and its cooling efficiency improves. Hence, the low energy efficiency of energy conversion for TEC is expected to be solved by employing the energy feedback technology proposed in this paper, which provides a new idea for high efficiency thermoelectric scheme.

A. Theoretical Basis of Energy Feedback System

The system can switch the H-bridge on and off by outputting PWM waves with different duty cycles to control the current. The waveform of the current without a filter rectifier circuit is presented in Fig. 5. Theoretically, the rectifier filter circuit can be removed to collect the reverse Seebeck voltage through the energy feedback circuit when the TEC is in the no-load state

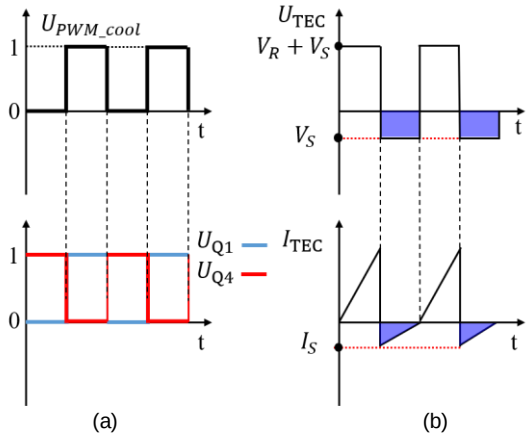

Fig. 5. Transient U/I variation in the PWM and TEC devices. (a) Waveform of the PWM signal and MOSFET voltage. (b) The voltage and current of a semiconductor refrigerator.

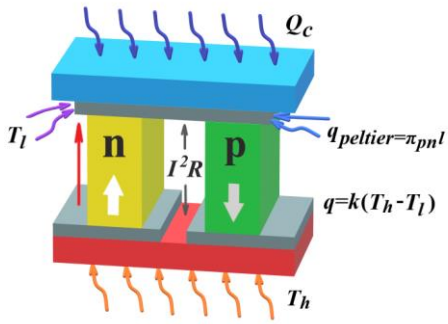

Fig. 6. Arm of the thermocouple.

shown in Fig. 5(b). In each cycle of the TEC in this state, it is used as a thermoelectric generator (TEG) to generate electricity and collect electric energy by taking advantage of the temperature difference between the two ends of the TEC (blue part in Fig. 5(b)). As a semiconductor heat pump, the applied voltage at both ends of each thermoelectric arm in the workshop should be equal to the drop-in voltage on it (V_R) plus the drop required for the reverse Seebeck voltage (V_S):

$$V = V_R + V_S = IR + S_{np}(T_h - T_l) \tag{3}$$

where S_{np}, T_h, and T_l are the Seebeck coefficient, and the temperatures at the hot and cold ends, respectively. The current loop allows the thermocouple arm to establish a temperature difference $\Delta T=T_h-T_l$ on both surfaces. According to the Peltier effect, heat transferred from the cold to the hot end of the device is $\pi_{np}I$. The thermocouple arm is shown in Fig. 6. Due to the temperature difference between the ends of the TEC, heat is transferred from the hot to the cold surface of the device. Suppose the total thermal conductivity of the device is K, then the thermal reflux is $K\Delta T$. In addition, owing to the internal resistance of the device, the corresponding joule heat is also generated and evenly transmitted to the cold and hot ends of the device. If the internal resistance of the device is R, the heat flowing into the hot end per unit time is $0.5I^2R$(J). Thus, the refrigeration device is considered a closed adiabatic system, and the heat balance of the cold end can be expressed by Equation 4.

$$COP = \frac{Q_c}{P} = \frac{S_{np}T_L I - \frac{1}{2}I^2R - K\Delta T}{I^2R + S_{np}\Delta TI} \quad (4)$$

where Q_c is defined as the heat absorbed by the TEC per unit time and P as the electric energy input per unit time. In the TEC refrigeration system designed with energy feedback, it is assumed that the period is $T=a+b$, where b is the no-load time of the TEC. Its cycle refrigeration coefficient is defined as

$$COP = \frac{aQ_c - bQ_g}{aP_c - bP_g} \quad (5)$$

where Q_c, Q_g, P_c, and P_g are the heat absorption at the cold end, the heat returns at the hot end, the input power, and the recovery power, respectively. Also, we know that

$$Q_g = S_{np}\Delta TI' + K\Delta T \quad (6)$$

$$P_g = \frac{S_{np}^2 \Delta T^2 R_1}{(R+R_1)^2} \quad (7)$$

By combining (5), (6), and (7), we have

$$COP_{feedback} = \frac{a(S_{np}T_L I - \frac{1}{2}I^2R - K\Delta T) - b(S_{np}\Delta TI' + K\Delta T)}{a(I^2R + S_{np}\Delta TI) - b(\frac{S_{np}^2\Delta T^2 R_1}{(R+R_1)^2})} \quad (8)$$

where R_1 is the load resistance and I' is the reverse Seebeck current when the TEC is in the no-load state.

$$I' = \frac{S_{np}\Delta T}{R} \quad (9)$$

Equations. (8) and (9) show that $COP_{feedback}$ can be adjusted by the value of the duty cycle in the system. Within a certain range, the higher the duty ratio of the output PWM wave signal is, the greater the current passing through TEC is. This means that the temperature difference in the TEC is greater when there is no load, but the time to recover the Seebeck electricity is also shorter.

The inequality is computed iteratively when the conventional coefficient (S_{np}, a, b, K) is limited to a finite value, and $COP_{feedback} > COP$ is established. This means that the cooling efficiency of the TEC is increased and energy is saved by the proposed TEC cooling process with energy feedback.

In practical application, there is often a more accurate parameter ψ to measure the working efficiency of TEC, and the calculation formula is described as follows:

$$\psi = \frac{exergy\_out}{exergy\_in} \quad (10)$$

Equation (10) is derived from exergy analysis [32], which defines ψ as the ratio of exergy output and exergy input, where the former is only a part of Q and the latter is the electrical power consumption P.

$$exergy\_in = P \quad (11)$$

$$exergy\_out = Q\left(\frac{T_h}{T_c} - 1\right) \quad (12)$$

Thus, ψ can be described as

$$\psi = \frac{Q}{P}\left(\frac{T_h}{T_c} - 1\right) \quad (13)$$

Submitting Eq. (4) into (13), we have the refrigeration efficiency of TEC with cycle modulation.

$$\psi = \frac{a(S_{np}T_L I - \frac{1}{2}I^2R - K\Delta T) - b(S_{np}\Delta TI' + K\Delta T)}{a(I^2R + S_{np}\Delta TI) - b(\frac{S_{np}^2\Delta T^2 R_1}{(R+R_1)^2})}\left(\frac{T_h}{T_c} - 1\right) \quad (14)$$

B. Circuit Design and Simulation

Fig. 4 shows an H-bridge circuit without the rectifier filter circuit. Q1 and Q4 are switched on and off via the PWM_COOL signal in the refrigeration mode. The duty cycle of the signal determines the effective current of the TEC. To verify the feasibility of the scheme, the designed energy feedback scheme was simulated using Multisim simulation software. To recover the reverse current when the MOSFET was turned off, the energy feedback circuit was turned on at both ends of the TEC. The energy feedback circuit was turned off when the H-bridge circuit was on and turned on when the H-bridge was off. Therefore, the switch circuit shown in Fig. 7 was designed in which the input to the PWM signal was controlled by Raspberry Pi. When the TEC power supply circuit was on, the TEC operated normally. When the circuit was disconnected, the TEC acted as a TEG while Seebeck electrical energy was generated and led out through the cooperative feedback circuit.

The simulation system was composed of three parts as shown in Fig. 7. Current control was realized by the H-bridge circuit. When the H-bridge circuit was turned off, the rectifier bridge circuit and the collaborative feedback circuit turned on. At the same time, owing to the large temperature difference within the TEC, Seebeck voltage was generated and extracted by the rectifier circuit. Thus, reverse Seebeck voltage was collected with the TEC without load. This energy can be used to power low-energy devices, such as sensors of system, through the voltage-stabilizing boost module to improve the efficiency of energy utilization of the TEC. The obtained simulation data in different duty cycles are listed in Table IV. An effective current of 24 μA with a peak voltage of 1.2 V and a duty cycle of 75% was generated when the load resistance was 3 Ω. The results show that energy feedback technology can be applied to TEC refrigeration to improve the efficiency of energy conversion.

TABLE IV
SIMULATION DATA FOR THE ENERGY FEEDBACK SYSTEM

Duty cycle	Supply Voltage	Reverse voltage	Reverse current
25%	12V	0.37V	16μA
50%	12V	0.76V	20μA
75%	12V	1.2V	24μA

TABLE V
TYPE SPECIFICATIONS OF THE MAIN DEVICES

Devices	Type specification
Raspberry Pi	4B
Temperature sensor	LM75
Current sensor	INA219
TEC	Bi_2Te_3
Solar panel	6V/1A
Battery	2800 mA/h
Relay	Digital control

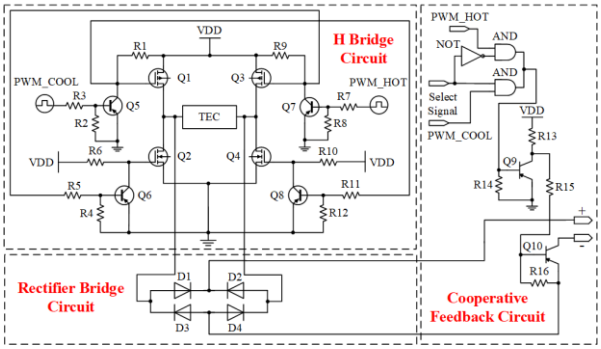

Fig. 7. Circuit diagram of temperature control and energy feedback system.

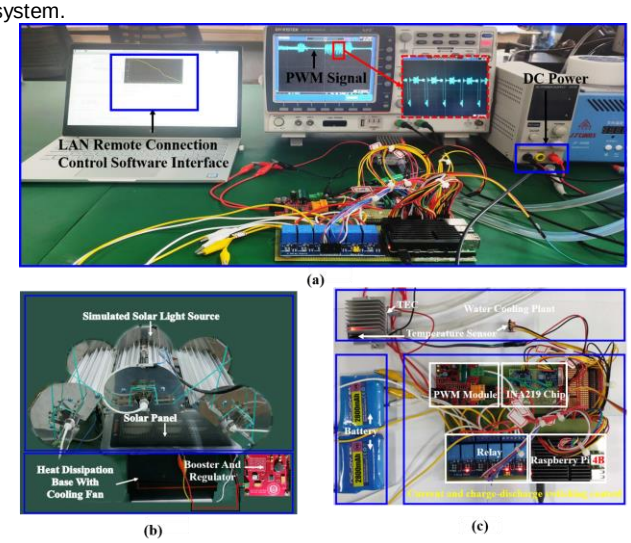

Fig. 8. (a) Experimental platform for the temperature control system. (b) Solar panel and simulated light source. (c) Detailed information on the proposed TEC temperature control system.

IV. Experimental Design

A. Design of Experimental Scheme

In proposed system, the PWM signal from Raspberry Pi 4B was used to control the current of the TEC refrigeration circuit. Temperature control was also exercised, where the improved PID temperature feedback regulation was a closed-loop control process used to adjust the output of the PWM signal of the MCU at the next instant by using temperature data from the previous instant. This requires that the temperature sensor communicates with the MCU. To realize intelligent and efficient switching of the state of the power supply, the magnitude of the electric current, and the charging and discharge currents of the two battery packs needed to be monitored in real time during the operation of the system.

The charging part consisted of two parts: normal power charging and solar panel charging. The latter requires a boost circuit and a charge protection circuit to assist the normal focus of the battery. The proposed experimental scheme for temperature control of the TEC [33] is shown in Fig. 8. The main devices and modules are listed in Table V, where the INA219, LM75, and other sensors communicated with the MCU using the I²C protocol. Raspberry Pi served as the control host. The experimental platform is shown in Figs. 8(a), (b), and (c). In Fig. 8(a), the output PWM wave signal is connected to

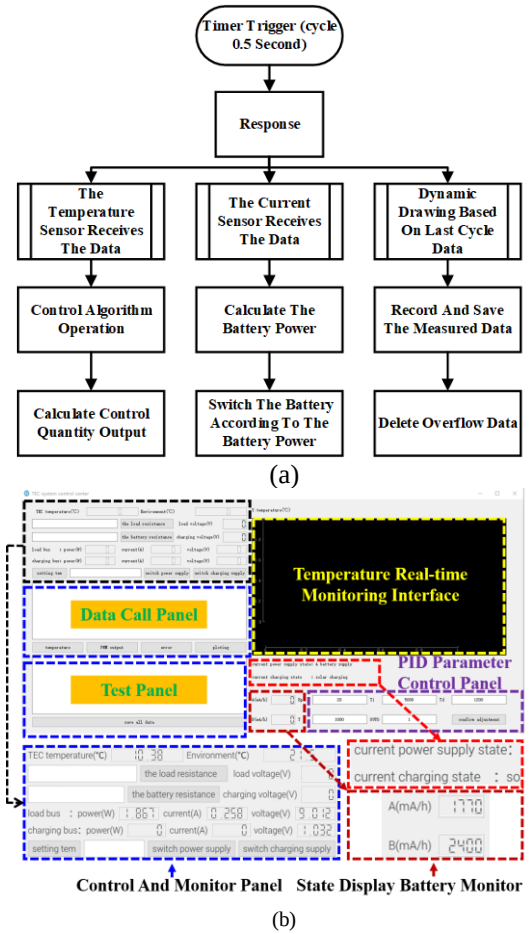

Fig. 9. (a) Multi-threading software. (b) Operational interface of software with traditional PID control algorithm.

the oscilloscope for real-time monitoring, and the system is charged by the solar panel through the DC power supply in Figs. 8(a) and (b). Detailed information on the wiring layout of the device is shown in Fig. 8(c). Due to the hysteresis of temperature regulation, the period of PWM control signal output by upper computer is set to 50 Hz, which is also the empirical value considering the current continuity.

The circuit-monitoring chip was employed to track the electric intensity and current. If the monitoring period was set to T(h), values of the measured current in the discharge group within n cycles were I_1, I_2, I_3, …, I_n (mA), and those in the charging group were i_1, i_2, i_3, …, i_n (mA). Then, the magnitudes of the charge and discharge of the battery in n cycles were as in (15) and (16), respectively.

$$Q_c = \sum_{k=1}^{n} \int_0^T i_k dt \tag{15}$$

$$Q_{disc} = \sum_{k=1}^{n} \int_0^T I_k dt \tag{16}$$

In the process of switching power supply, the MCU's power supply switching command was implemented by digital control relay. In this power management, an intelligent charge and discharge management scheme based on photovoltaic charging and supplemented by power charging is proposed. Combined with the efficient energy feedback mechanism for TEC, it provides a new solution for some application scenarios with heat dissipation or heating demand lacking of energy supply, such as space and seabed.

B. Design of Control Software

In the proposed TEC temperature control system, a complete upper computer system is needed that satisfies the following requirements:

- complete UI interface;
- stable communication with sensor and hardware;
- real-time monitoring and display of data;
- ability to set TEC surface temperature and control;
- ability to adjust PID in the control process;
- stable and fast operation;
- ability to save and export historical data.

The PYQT5 is a toolkit for creating GUI applications that is a successful fusion of Python and the QT library. Programs written in PYQT5 run well in a Linux environment. To build a visual interface on Raspberry Pi, the system used PYQT5 for interface development. A real-time data display and graphics interface was developed by using PYQT and its graph library. Moreover, due to the GPIO (general-purpose input/output) interface of Raspberry Pi, it could output digital signals to control the MOSFETs and relay, and used I^2C to communicate with the sensor to obtain the data. The data were then integrated and rendered in the software. This system was developed using tools in Python's PyQt5 library. Owing to the large amount of data that needed to be processed, the system was divided into three threads. As shown in Fig. 9(a), the first thread was used to obtain data from the temperature sensor to control the operation of the algorithm and output the control signal. The second thread was used to monitor the power and current, where these data were used for calculation and judgments. The digital signal was output to the relay to switch the power supply. The third thread was used for dynamic drawing and data display, and executed the relevant operations when receiving such instructions such as setting the TEC temperature, switching the power supply, adjusting the parameters of PID, and saving and exporting data. According to these requirements, the control software was designed using the UI shown in Fig. 9(b).

V. Results and Discussion

In the proposed temperature control system, the refrigeration (heating) limit of the temperature control platform needed to be known first. Therefore, the PWM duty cycle was set to 100%, and functioned in refrigeration and heating modes, respectively. The change in the transient temperature under different modes of operation was obtained as shown in Fig. 10(a). The variation of time and TEC temperature in the heating mode is represented by red curve, while the one in the refrigeration mode is represented by blue curve with time scale unit of 0.5s. It is clear that the range of temperature control of 1.437 ℃ to 60.187 ℃ was achieved by cooling water when the maximum output current was 3.1 A at an ambient temperature of 22 ℃. This is a considerably wide range without pollution or noise.

To evaluate the energy utilization efficiency of our proposed system, COP and ψ were calculated according to Equations (8)-(14) based on experimental data, which were illustrated in Fig. 10(b). It can be seen that when the temperature difference was 44.3K, COP was increased from 4.2 to 5.08 by changing the duty cycle a from 1 to 0.2, and the corresponding efficiency ψ was also increased from 0.65 to 0.79, showing a significant improvement.

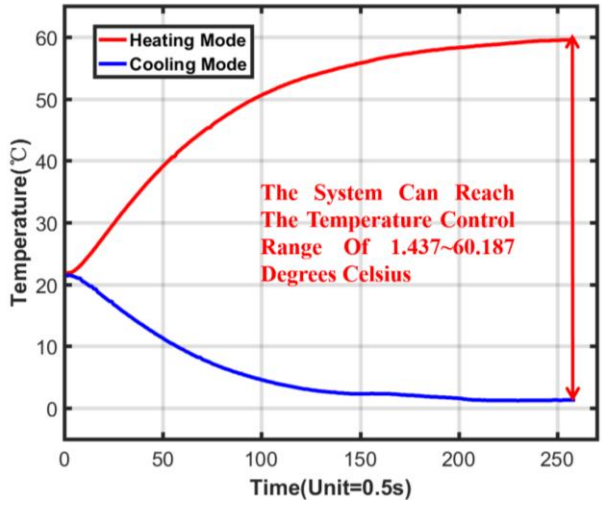

(a)

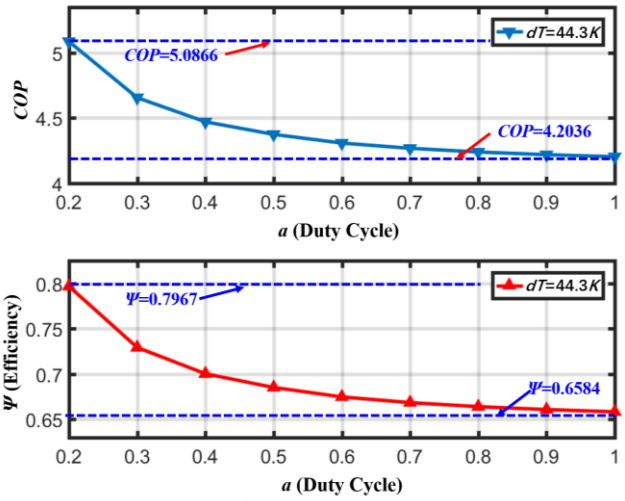

(b)

Fig. 10. (a) Cooling (heating) capacity of temperature control system. (b) a (duty cycle) and *COP* (refrigeration coefficient), ψ (refrigeration efficiency) curve diagrams.

At the last time, to evaluate the optimized algorithm, it was applied along with the conventional control algorithm to the same hardware system as shown in Fig. 8, when the ambient temperature was 22 ℃ and the target temperature was 10 ℃. The trend of temperature, detailed information on the load and charging circuits, parameters of the PID, and ambient temperature could be read from the software in real time. A series of functions could thus be implemented, such as monitoring current in the circuit, controlling the status of the battery, and controlling the temperature. To compare the groups of data more intuitively, they were exported and plotted as shown in Fig. 12(a) and (c). The red line (including the dotted line) represents the optimized algorithm and the black line represents the conventional algorithm. The time unit of all abscissa in the figure is 0.5s, that is, each scale unit in the abscissa represents the sampling interval of 0.5s. The data show that the optimized temperature control algorithm had significant advantages over the conventional PID temperature control algorithm. The convergence state is defined when the temperature error is controlled within the range of ±0.35℃ of

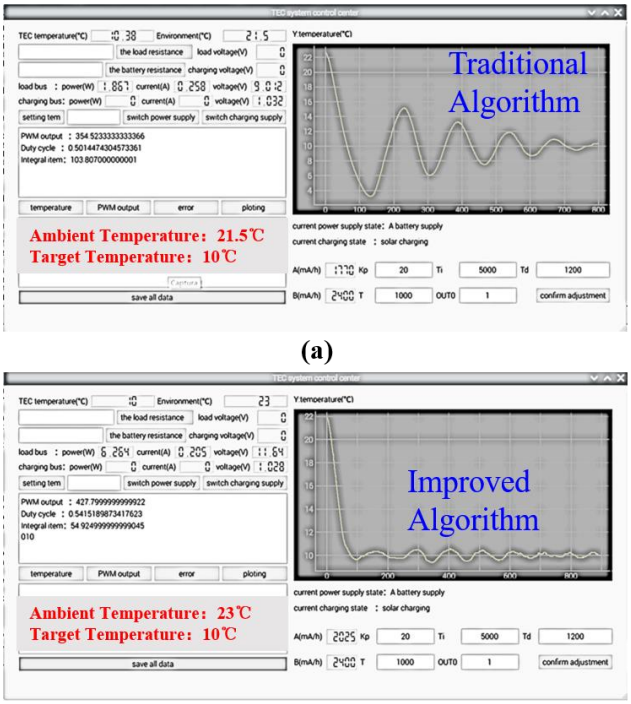

Fig. 11. Interface of upper computer. (a) The temperature is set to 10 ℃ for cooling in the traditional algorithm. (b) The temperature is set to 10 ℃ for cooling in the improved algorithm.

the target temperature. According to the convergence condition, the convergence time with the optimized PID algorithm was only 30.5 s, whereas it took 287 s for the conventional temperature control algorithm to reach the same accuracy. In comparison, when the ambient temperature was 22 ℃ and the set temperature was 10 ℃, the optimized temperature control algorithm was 256.5 s faster than the conventional one. When the ambient temperature was 22 ℃ and the set temperature was 45 ℃, Fig. 12(b) and (d) were obtained. Supposing that the error was 1.1 ℃, the time need for control by the improved PID algorithm control was 31 s while the conventional algorithm needed 249 s to reach the same precision. In fact, the convergence time in the cooling or heating mode can also be adjusted by modifying parameters *P, I, D, T* in the two-stage PID regulation, and the time of which can be even faster in the proposed system.

Table VI gives the performance comparison of our proposed system with other control groups. Data of the first and the second groups in Table VI were obtained from [22,24] and compared with data obtained by the temperature control system proposed in this paper. Control group A achieved a range of temperature control of 5-55 °C and control group B achieved that of 8.3-40.3 °C with the addition of 6 A of current. However, the proposed system achieved a range of temperature control of 1.437-60.187 ℃ with 3 A of additional current. In terms of speed of regulation, it was used to regulate a temperature difference of 13 ℃ for 30.5 s. It was also superior to the other methods in terms of control accuracy, 0.1 ℃. The most significant difference between the proposed system and the other control groups was in the application of energy feedback technology, which enabled the TEC to recover the reverse Seebeck electrical energy to drive the sensor while operating to

TABLE VI
COMPARISON OF SYSTEM FUNCTIONS

Group	Control group A	Control group B	**Proposed system**
Materials	Bi_2Te_3	Bi_2Te_3	**Bi_2Te_3**
Arithmetic	Conventional PID	Conventional PID	**Improved PID**
Energy feedback	N	N	**Y**
Control range of T(℃)/I_{max}(A)	5~55/ Unavailable	8.3-40.3 /6A	**1.437~60.19 /3.1A**
Time of adjustment (s)/ ΔT(℃)	Unavailable	800s/11	**30.5s/13**
Accuracy(℃)	0.5	Unavailable	**0.1**

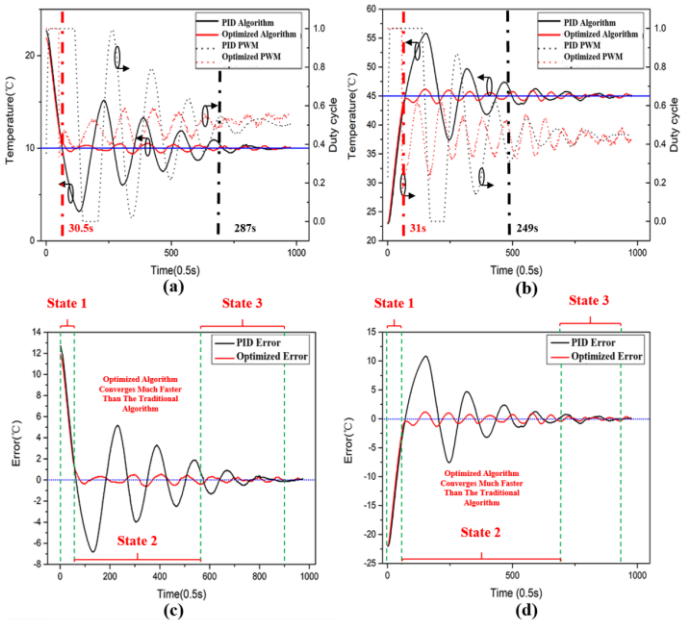

Fig. 12. Analysis of temperature data. (a) Temperature was set to 10 ℃ for cooling. (b) Temperature was set to 45 ℃ for heating. (c) Variation in error in cooling process. (d) Variation in error in heating process.

improve the efficiency of energy utilization. The efficiency of refrigeration can also be modulated by adjusting the duty ratio. With the proposed efficient TEC temperature control technique, the issues of non-linearity and hysteresis in temperature control can be completely solved, the method of which is also can be used in rapid temperature response scenarios such as firing materials and preservation of medical drugs.

VI. CONCLUSION

In this paper, a TEC temperature control system was proposed with a complete and interactive upper computer system. An improved temperature control algorithm that can quickly and accurately control the surface temperature of the TEC was obtained. Compared with the control time of 287 s by the conventional method, the proposed temperature control system had a control time of 30.5 s with an accuracy of 0.1 ℃, and an error of only ±0.35 ℃ while targeting a temperature of 10 ℃ at an ambient temperature of 22 ℃. Also, a wide range of temperature control from 1.437 ℃ to 60.187 ℃ was implemented when the ambient temperature is 22 ℃ and the maximum input current is 3 A. Based on the energy harvesting mechanism of TEC, the proposed work may help resolve

energy challenges in power portable equipment, space power supply, low-power industrial control and automotive electronics.

REFERENCES

[1] R. Edwards and C. Gould, "Review on Micro-Energy Harvesting Technologies," in Proc. 51st Int. Universities Power Engineering Conf. (Upec), 2016.

[2] F. Felgner, L. Exel, M. Nesarajah, and G. Frey, "Component-Oriented Modeling of Thermoelectric Devices for Energy System Design," IEEE Trans. on Industrial Electronics., vol. 61, no. 3, pp. 1301-1310, Mar. 2014.

[3] J. H. Li, X. R. Zhang, C. Zhou, J. G. Zheng, D. S. Ge, and W. H. Zhu, "New Applications of an Automated System for High-Power LEDs," IEEE-Asme Trans. On Mechatronics., vol. 21, no. 2, pp. 1035-1042, Apr. 2016.

[4] N. Wang, H. W. Li, C. Ding. et al., "A Double-Voltage-Controlled EffectiveThermal Conductivity Model of Graphene for Thermoelectric Cooling," IEEE Trans. on Electron Devices., vol. 65, no. 3, pp. 1185-1191, Mar. 2018.

[5] K. Xie and M. C. Gupta, "High-Temperature Thermoelectric Energy Conversion Devices Using Si-Ge Thick Films Prepared by Laser Sintering of Nano/Micro Particles," IEEE Trans. on Electron Devices., vol. 67, no. 5, pp. 2113-2119, May. 2020.

[6] F. Kaplan, M. Said, S. Reda and A. K. Coskun, "LoCool: Fighting Hot Spots Locally for Improving System Energy Efficiency," IEEE Trans. on Computer-Aided Design of Integrated Circuits and Systems., vol. 39, no. 4, pp. 895-908, April. 2020.

[7] S. A. Al-Shehri, "Cooling Computer Chips with Cascaded and Non-cascaded Thermoelectric Devices," Arabian Journal for Science and Engineering., vol. 44, no. 11, pp. 9105-9126, Nov. 2019.

[8] B. Alexandrov, O. Sullivan, W. J. Song, S. Yalamanchili, S. Kumar, and S. Mukhopadhyay, "Control Principles and On-Chip Circuits for Active Cooling Using Integrated Superlattice-Based Thin-Film Thermoelectric Devices," IEEE Trans. on Very Large Scale Integration Systems., vol. 22, no. 9, pp. 1909-1919, Sep. 2014.

[9] J. Y. Long, D. W. Li, S. O. Memik, and S. Ulgen, "Theory and Analysis for Optimization of On-Chip Thermoelectric Cooling Systems," IEEE Trans. on Computer-Aided Design of Integrated Circuits and Systems., vol. 32, no. 10, pp. 1628-1632, Oct. 2013.

[10] H. H. Saber, S. A. AlShehri, and W. Maref, "Performance optimization of cascaded and non-cascaded thermoelectric devices for cooling computer chips," Energy Conversion and Management., vol. 191, pp. 174-192, Jul. 2019.

[11] N. F. Guler and R. Ahiska, "Design and testing of a microprocessor-controlled portable thermoelectric medical cooling kit," Applied Thermal Engineering., vol. 22, no. 11, pp. 1271-1276, Aug. 2002.

[12] A. Rahmani, R. H. P. Rezaee, and N. Kordani, "Smart Portable Cryotherapy System Rephrased I.E. With Controlled Thermoelectric Cooling Modules for Medical Applications," Iium Eng J., vol. 19, no. 1, pp. 117-128, 2018.

[13] T. Tokiwa et al., "A Palm-Sized Cryoprobe System With a Built-In Thermocouple and Its Application in an Animal Model of Epilepsy," IEEE Trans. on Biomedical Engineering., vol. 66, no. 11, pp. 3168-3175, Nov. 2019.

[14] Hato, A. Tsukamoto, and K. Tanabe, "Portable Cryostat With Temperature Control Function for Operation of HTS-SQUID at a Higher Slew Rate," IEEE Trans. on Applied Superconductivity., vol. 29, no. 5, Aug. 2019.

[15] C. Li, D. Jiao, J. Z. Jia, F. Guo, and J. Wang, "Thermoelectric Cooling for Power Electronics Circuits: Modeling and Active Temperature Control," IEEE Trans. on Industry Applications., vol. 50, no. 6, pp. 3995-4005, Nov-Dec. 2014.

[16] H. Zhang, Z. Guo and Y. Lu, "Enhancement of Hot Spot Cooling by Capped Diamond Layer Deposition for Multifinger AlGaN/GaN HEMTs," IEEE Trans. on Electron Devices., vol. 67, no. 1, pp. 47-52, Jan. 2020.

[17] Q. Tian et al, "Efficient Heat Dissipation Study of High-Power W -Band Sheet Beam Extended Interaction Oscillator," IEEE Trans. on Electron Devices., vol. 65, no. 11, pp. 5075-5081, Nov. 2018.

[18] S. Prasad Bag, X. Hou, J. Zhang, S. Wu and J. Wang, "Negative/Positive Electrocaloric Effect in Single-Layer $Pb(Zr_xTi1–x)O_3$ Thin Films for Solid-State Cooling Device," IEEE Trans. on Electron Devices., vol. 67, no. 4, pp. 1769-1775, April. 2020.

[19] A. Mironova, B. Haus, A. Zedler, and P. Mercorelli, "Extended Kalman Filter for Temperature Estimation and Control of Peltier Cells in a Novel Industrial Milling Process," IEEE Trans. on Industry Applications., vol. 56, no. 2, pp. 1670-1678, Mar-Apr. 2020.

[20] N. Wang, C. Gao, C. Ding, H. Z. Jia, G. R. Sui, and X. M. Gao, "A Thermal Management System to Reuse Thermal Waste Released by High-Power Light-Emitting Diodes," IEEE Trans. on Electron Devices., vol. 66, no. 11, pp. 4790-4797, Nov. 2019.

[21] N. Wang, X. C. Li, and J. F. Mao, "Improvement of Thermal Environment by Thermoelectric Coolers and Numerical Optimization of Thermal Performance," IEEE Trans. on Electron Devices., vol. 62, no. 8, pp. 2579-2586, Aug. 2015.

[22] Sundayani et al., "PID Temperature Controlling of Thermoelectric Based Cool Box," in Proc. Int. Conference on Control, Electronics, Renewable Energy and Communications (Iccrec), 2017, pp. 236-240.

[23] W. S. Woodward, "Achieve precision temperature control with TEC Seebeck-voltage sampling," Electrical Design News., vol. 53, no. 24, pp. 60-62, Nov. 2008.

[24] H. Huang, S. M. Fu, P. Zhang, and L. K. Sun, "Design of a Small Temperature Control System Based on TEC," in Proc. 9th Int. Symposium on Computational Intelligence and Design (Iscid), 2016, vol. 1, pp. 193-196.

[25] Y. Sargolzaeiaval et al., "Flexible thermoelectric generators for body heat harvesting - Enhanced device performance using high thermal conductivity elastomer encapsulation on liquid metal interconnects," Applied Energy., vol. 262, Mar. 2020.

[26] T. Watanabe et al., "A Scalable Si-based Micro Thermoelectric Generator," in Proc. IEEE Electron Devices Technology and Manufacturing Conf. (Edtm), 2017, pp. 86-87.

[27] B. Wu, Y. Guo, C. Y. Hou, Q. H. Zhang, Y. G. Li, and H. Z. Wang, "High-Performance Flexible Thermoelectric Devices Based on All-Inorganic Hybrid Films for Harvesting Low-Grade Heat," Advanced Functional Materials., vol. 29, no. 25, Jun. 2019.

[28] S. D. Xu et al., "High-Performance PEDOT: PSS Flexible Thermoelectric Materials and Their Devices by Triple Post-Treatments," Chemistry of Materials., vol. 31, no. 14, pp. 5238-5244, Jul. 2019.

[29] J. B. Yan, X. P. Liao, D. Y. Yan, and Y. G. Chen, "Review of Micro Thermoelectric Generator," J Microelectromech S., vol. 27, no. 1, pp. 1-18, Feb. 2018.

[30] A. B. Zhang and B. L. Wang, "Temperature and electric potential fields of an interface crack in a layered thermoelectric or metal/thermoelectric material," International Journal of Thermal Sciences., vol. 104, pp. 396-403, Jun. 2016.

[31] G. Engelmann, M. Laumen, J. Gottschlich, K. Oberdieck, and R. W. De Doncke,"Temperature-Controlled Power Semiconductor Characterizati-on Using Thermoelectric Coolers," IEEE Trans. on Industry Applications., vol. 54, no. 3, pp. 2598-2605, May-Jun. 2018.

[32] S. Manikandan, S. C. Kaushik, and K. Anusuya, "Thermodynamic modelling and analysis of thermoelectric cooling system," in *Int. Conf. Energy Effic. Technol. Sustain. ICEETS.*, 2016, pp.685-693, doi: 10.1109/ICEETS.2016.7583838.

[33] Thermonamic Corporation, Specification of Thermoelectric Module TEC1-24112, http://www.thermonamic.com/TEC1-24112-English.PDF.

Ning Wang was born in 1984. He received the M.S. and Ph.D. degrees in microelectronic from Xidian University, Xi'an, China, in 2009 and 2012, respectively. From 2012, he joined China North Industries Group Corporation General Electronic-s Group, Suzhou, China, as a R&D engineer and Project Leader. From 2013 to 2015, he was a postdoctoral researcher at Shanghai Jiao Tong University, Shanghai. Since 2015, he has been a Faculty Member with University of Shanghai for Science and Technology, Shanghai, where he is currently an associate professor. His current research interests include thermoelectric energy conversion, waveguide in terahertz and vortex electromagnetic wave.

Zhou-Xiao Liu was born in 1996. He received the Bachelor degree in electronic Science and Technology from University of Shanghai for Science and Technology in 2018. He is pursuing a Master of Engineering in Optical Engineering from University of Shanghai for Science and Technology. His research interests includes thermoelectric energy harvesting and energy recovering.

Can Ding was born in Huaibei, China, in 1989. He received the bachelor's degree in microelectronics from Xidian University, Xi'an, China, in 2009. and the Ph.D. degree from Macquarie University, Sydney, NSW, Australia, in 2015. From 2015 to 2017, he was a Post-Doctoral Research Fellow at the University of Technology Sydney (UTS), Sydney, where he is currently a Lecturer with the Global Big Data Technologies.

Jian-Nan Zhang was born in 1996. He received the Bachelor degree in electronic Science and Technology from University of Shanghai for Science and Technology in 2019. He is pursuing a Master of Engineering in Optical Engineering from University of Shanghai for Science and Technology. His research interests include thermoelectric energy harvesting and maximum power point tracking.

Guo-Rong Sui was born in 1974. He received the Ph.D degrees in optical engineering from University of Shanghai for Science and Technology, Shanghai, China, 2008. From 2008, he has been a faculty Member with University of Shanghai for Science and Technology, Shanghai, where he is currently an associate professor. His current research interests include high-speed semiconductor device, integrated optics device and optical-electrical detection.

Hong-Zhi Jia was born in 1968. He received the B.S. degree in microelectronic from Beijing Institute of Technology, Beijing, China in 1990, and Ph.D. degrees from Xi 'an optical precision machinery research institute of Chinese academy of sciences, Xi'an, China, in 2000.

Since 2002, he has been a Faculty Member with University of Shanghai for Science and Technology, Shanghai, where he is currently a professor. His current research interests include fiber optical sensors and photodetector.

Xiu-Min Gao was born in 1978. He received his PhD degree from Shanghai Institute of Optics and Fine Mechanics (SIOM) in 2006, and joined University of Shanghai for Science and Technology (USST) in 2017. He is leader of several research Programs including National Natural Science Foundation of China, National key research and development plan. He has published more than 60 papers in journals such as Nature Communications, Scientific Reports, and Applied Optics. He obtained more than 50 patents, and his several research achievements have been industrialized. His current research includes instruments and meters, smart sensing technology, optical engineering, and precision measurement.